

A Study of 1-dot Latent Image Potential

Kouichi Aizawa
Yoshihiro Ueno
Motohiro Takeshima

1. Introduction

Color printers and digital copiers are the main types of image information output devices and are classified according to the technology they employ, either ink jet technology or electrophotography. In the future, the use of ink jet technology is expected to increase for low-end home-use devices, while the use of electrophotographic technology is predicted to increase for applications that require high speed. However, better image quality is required of electrophotographic technology. Image quality includes such criteria as resolution, gradation and image density, but resolution is regarded as most important. At present, the resolution capabilities of commercially available electrophotographic devices range widely from 600 dpi (dots per inch) to 1,200 dpi or 2,400 dpi. The future trends toward colorization and digitization present the technical challenge of providing even higher levels of resolution.

In order to enhance the level of resolution, manufacturers of devices such as printers and copiers and manufacturers of materials such as photoconductors, toners and exposure lights have analyzed the factors that determine the resolution and have improved the photoelectric processes of charging, exposing, developing, transferring and fusing and have also improved the photoconductive materials used in photoconductor drums. Fuji Electric has also been moving forward with the development of high resolution photoconductors capable of forming electrical latent images with good reproducibility on a photoconductor. However, electrophotographic processes are complex and, at the present point in time, it is difficult to clearly identify which factors determine resolution quality.

The direct measurement of the static latent image, which is believed to have a large effect on the degree of resolution, has been proposed but there is no suitable way to measure the latent image on a photoconductor drum.⁽¹⁾

Simulation of the formation of a latent image has been attempted by Watanabe⁽²⁾ and Chen,^{(3) - (5)} however, these simulated results have not been directly compared to the latent image on a photoconductor.

In order to analyze the factors that determine the degree of resolution, Fuji Electric has developed a new evaluation device that measures the 1-dot latent image potential using a micro-area surface potential probe (MASPP), and has investigated the effect that changes in the organic photoconductor (OPC) material, and the layer structure have on latent image formation.

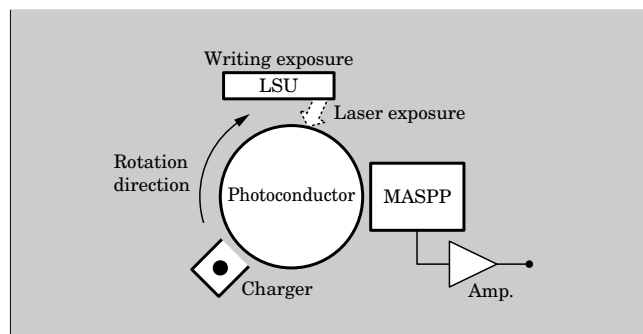
This paper describes in detail the principles of the MASPP-based latent image measurement and describes the relationships between the interpretation of the MASPP signal and electrophotographic properties. It is the authors' hope that this paper will contribute to improved photographic technology in the future.

2. 1-dot Latent Image Potential Measurement Device

2.1 Configuration of the latent image measurement device

The measurement device consists of a charging stage, an exposure light for writing, and the MASPP (see Fig. 1). A commercially available laser scan unit (LSU) for a printer is used as the writing exposure light. The LSU writes a 1-dot-wide line in the axial direction on a photoconductor that has been charged to a desired surface potential V_0 . Then, the written area is moved to the location of the MASPP and the potential of the micro-area is measured. At this time, the latent image profile can be acquired by taking multiple measurements, with a measurement step size of several tens of μm , of the micro-area potential around the periphery of the photoconductor.

Fig.1 Latent image potential measurement system



2.2 MASPP mechanism

The MASPP operates⁽⁶⁾ by detecting, as an induced current, the change in surface charge due to light decay of the photoconductor, and Fig. 2 shows the concept of the MASPP.

The surface of a charged photoconductor is exposed by a detection laser through a transparent electrode, which is located parallel to and approximately 1 mm from the photoconductor surface.

The photoconductor exposed by the detection laser undergoes light-decay, thereby changing the capacitance between the photoconductor and the transparent electrode and generating an induced current which is proportional to the change in surface charge of the photoconductor. The MASPP outputs a signal which is the amplified value of this induced current.

Figure 3 shows the measured values and a curve calculated according to a pulse function to be described later.

In the case where exposure from the detection laser nearly neutralizes the surface charge on the photoconductor, the size of the induced current will depend on the surface potential prior to exposure from the detection laser and the light decay characteristics of the photoconductor. Based on this relationship, by back-calculating the surface potential, it is possible to

measure the surface potential in the area that has been exposed by the detection laser. Fuji Electric has miniaturized the beam size of this detection laser to a diameter of approximately 10 μm , thereby enabling measurement of the surface potential at a micro-area.

2.3 Measurement of the latent image potential

Based on the results of various studies, the time for measuring the surface potential at a specific point by MASPP has been set to 650 ms. Figure 4 shows the MASPP signal obtained under this condition when a negatively charged multilayer OPC on which a latent image is formed is scanned at a 30 μm pitch.

Fifty-five different points are scanned, and the latent image potential profile can be obtained from this signal by calculating the change in charge due to exposure from the detection laser, and then converting that value into the surface potential.

In Fig. 4, the time required to measure the 1st to 55th points on the photoconductor surface was 35.75 seconds. Because the photoconductor has dark decay, this time must be reduced as much as possible, but present-day current measurement systems require approximately 200 ms for signal acquisition by detection laser exposure, approximately 100 ms to change the position by rotating the drum, and 100 to 300 ms to dissipate vibrations of the measurement system due to rotation and stopping. Accordingly, a further reduction of the measurement time would be difficult to accomplish at present.

Fig.2 Principle of MASPP operation

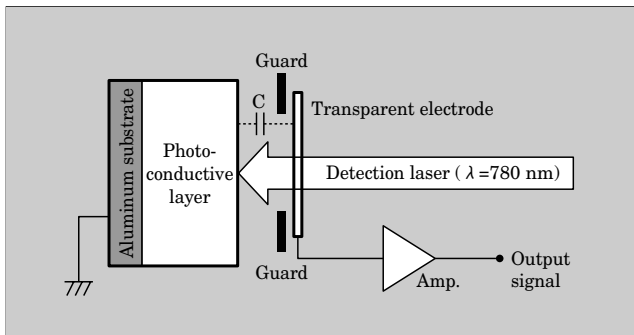
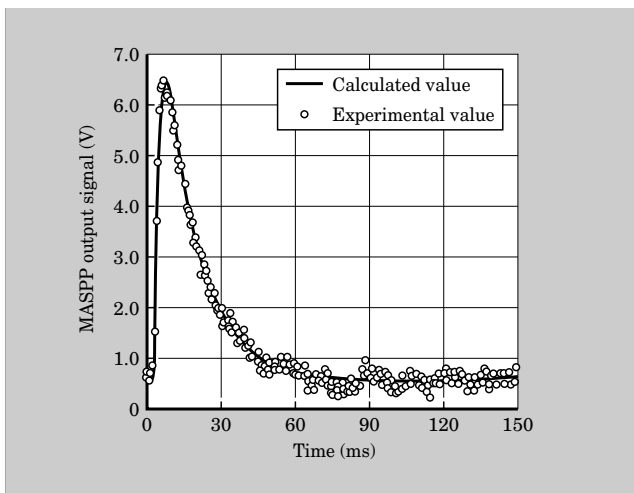


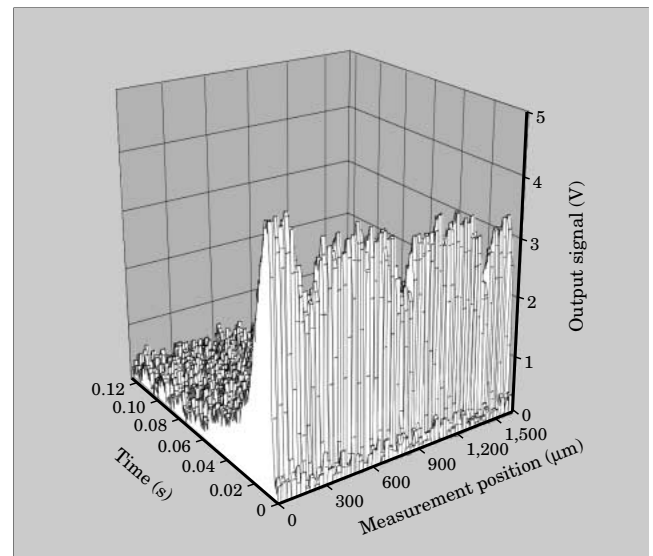
Fig.3 MASPP output signal



2.4 MASPP output signal

Examination of the MASPP output signal in response to detection laser exposure shows that the output signal can be approximated by the pulse function of Equation (1) (see Fig. 3). The signal can be approximated by Equation (1), and is independent of the layer structure and electronic properties of the

Fig.4 Example of MASPP signal



photoconductor and the polarity of the discharge.

$$S = S_{bg} + A \left\{ 1 - \exp\left(-\frac{t-t_0}{k_1}\right) \right\} \exp\left(-\frac{t-t_0}{k_2}\right) \dots\dots(1)$$

In the above equation, S is the MASPP output signal, S_{bg} is the offset value of the signal, t is time, and A , t_0 , k_1 and k_2 are constants.

Each parameter in the above equation can be determined by curve fitting the MASPP signal according to Equation (1).

The results of experiments about the correlations between various electronic properties of the photoconductor and numerical values of Equation (1) are described below. In anticipation of the capability to deduce the level of resolution even without measuring the latent image profile, analyses were conducted to clarify these correlations.

2.5 Charge retention and signal offset value (S_{bg})

Samples having different dark charge retention rates V_{k5} (charge retention after 5 seconds) were prepared in a negatively charged multilayer OPC. Measurements were taken at the initial charge potential of -500 V, and S_{bg} was obtained by curve fitting Equation (1) according to the obtained MASPP signal. Figure 5 shows the correlation between S_{bg} and the dark charge retention rate. S_{bg} increases as V_{k5} is made smaller (as the dark decay becomes larger). This phenomenon can be understood because the MASPP mechanism outputs a signal proportional to the change in charge of the photoconductor per unit time.

2.6 Maximum signal amplitude and sensitivity

Negatively charged OPC samples having different light sensitivities were prepared, and with the surface potential set to -600 V, the MASPP signal during exposure from the detection laser was analyzed. The maximum amplitude of the MASPP signal during exposure from the detection laser was S_{max} .

The correlation between S_{max} and light sensitivity E_{200} (quantity of light exposure required for the surface potential to decay from -600 V to -200 V) is shown in Fig. 6.

Similar to the case of S_{bg} , this correlation can also be understood based on the MASPP mechanism. A photoconductor that is highly light sensitive is thought to exhibit a large S_{max} due to its large change in charge per unit time while exposed to light.

2.7 Signal peak time and charge mobility

The correlation between the time from exposure by the detection laser until the MASPP signal reaches its maximum (t_{peak}) and charge mobility of the charge transport layer (CTL) is shown in Fig. 7. As the CTL charge mobility increases, t_{peak} becomes smaller. This phenomenon is due to the correlation between t_{peak} and the transit time of charges that move in the CTL and also to the correlation between transit time and charge

Fig.5 Correlation between charge retention and offset value

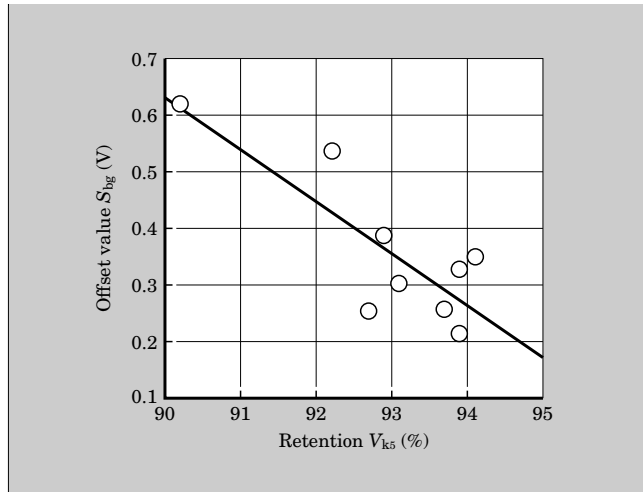
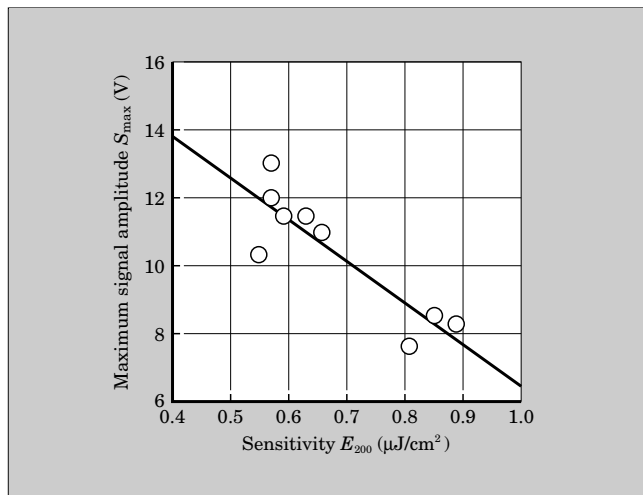


Fig.6 Correlation between sensitivity and maximum signal amplitude



mobility. The measured OPCs had identical thicknesses and charge potentials.

2.8 Change in charge and surface potential

Measurement by MASPP detects the change per unit time in the surface charge of a photoconductor. Consequently, the total change in charge can be calculated by integrating the MASPP signal generated by exposure to the detection laser. As has been described above, because the MASPP output signal contains both a component due to dark decay and a component due to light decay, the dark decay portion must be excluded during integration. Figure 8 shows the integrated signal value (Σ) for various values of initial charge potential V_0 on a negatively charged multilayer OPC.

The surface potential is computed by generating this type of calibration curve for each photoconductor that is measured. The static latent image profile is generated by computing the surface potential, using this calibration curve, from the change in charge

Fig.7 Correlation between charge mobility and maximum signal time

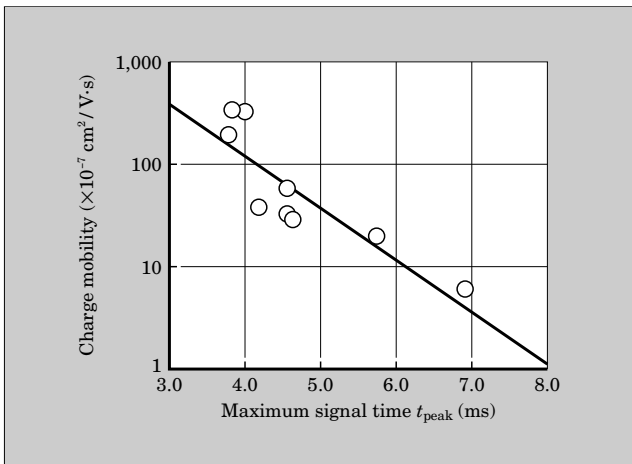
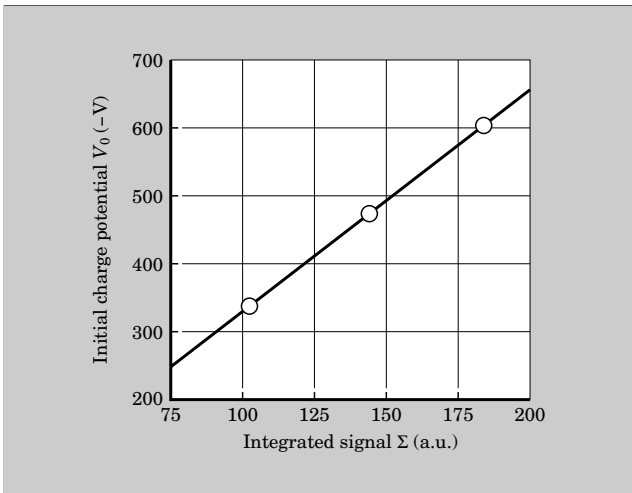


Fig.8 Correlation between integrated signal and initial charge potential



caused by exposure from the detection laser.

2.9 Latent image potential obtained by the 1-dot latent image measurement device

Figure 9 shows an example of the 1-dot latent image potential obtained with this device in the case of a negatively charged multilayer OPC.

In order to obtain the shape of the latent image potential, the potential is repeatedly measured 17 times with the MASPP at different positions. As described above, 650 ms are required for each MASPP measurement and therefore approximately 11 seconds elapsed from the 1st measurement point until the final 17th measurement point. Moreover, due to constraints of the device, 3 seconds are required from the time at which writing is performed until the time at which MASPP measurement begins. In the graph of Fig. 10, the vertical axis is the same as in Fig. 9 and the horizontal axis shows the time (t_m) that elapses after a 1-dot line has been written until the MASPP measurement is performed. In Figs. 9 and 10, there is an

Fig.9 1-dot latent image profile

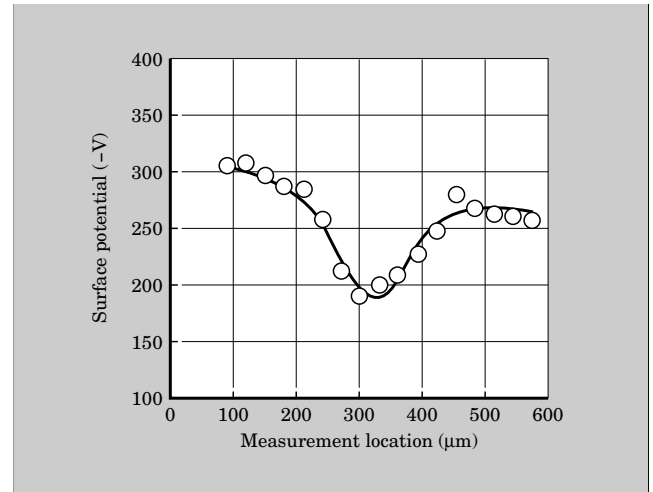
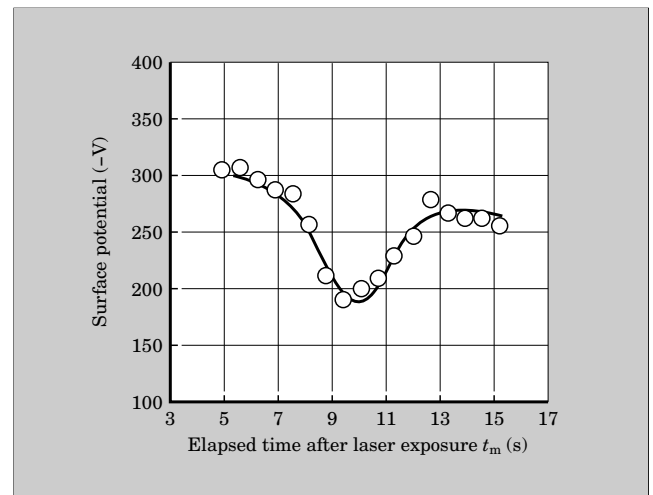


Fig.10 Elapsed time after writing and latent image potential



approximately 50 V difference in surface potential between the initial measurement point and final measurement point, and the latent image profile has an overall downward slope from left to right. In this system, because it is not possible to measure each point simultaneously, the time that elapses after writing will be different for each point, and this is the reason for the downward slope from left to right in the latent image profile obtained with this device.

3. Experimental Results

3.1 Measurement conditions

While the photoconductor drum is rotated at a speed of approximately 5 r/min, the drum surface is uniformly charged to the range of about ± 500 to ± 700 V. Then, an LSU having a dot width of approximately $80 \mu\text{m}$ at a strength of e^{-2} times its maximum strength, or if not specified, at an exposure power of 0.28 mW, writes a 1-dot-wide line, and the latent image potential is measured by MASPP with a measurement step size of $30 \mu\text{m}$. The width of the latent

Fig.11 Definition of surface potential width and depth

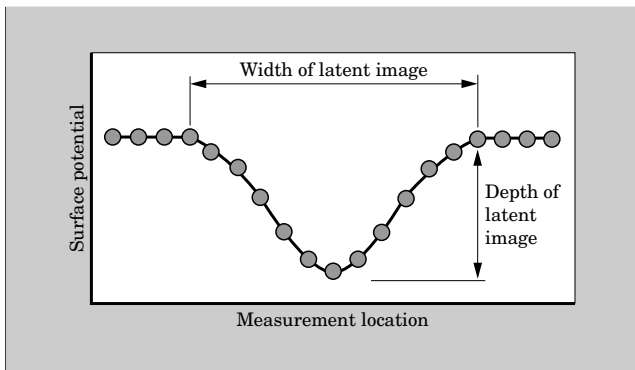


Fig.12 Writing light strength dependency of latent image

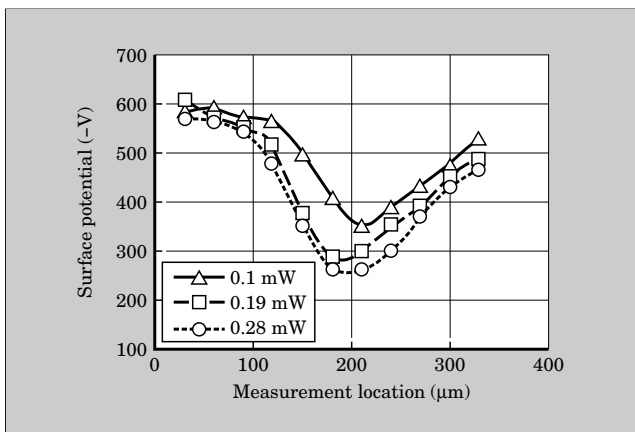


image in these experimental results indicates the width of the change in surface potential as shown in Fig. 11.

3.2 Exposure power dependency of the latent image

Figure 12 shows the change in latent image shape on a negatively charged multilayer OPC in the case where LSUs of various exposure powers are used to write a 1-dot-wide line. An increase in exposure power causes the latent image to become deeper and wider. This figure is in agreement with the generally known result that image density and line width increase with greater exposure power.

These results are important because they suggest that this measurement of a latent image profile is similar to the actual static latent image profile in an electrophotographic process.

3.3 Comparison of negatively charged OPC and positively charged OPC

Latent image potentials were measured for a negatively charged OPC and a positively charged OPC. Results of the measured latent image potentials are shown in Figs. 13 and 14.

Each OPC has the following layer configuration:

- (1) Negatively charged (multilayer) OPC: Aluminum substrate / charge generation layer (CGL) / CTL (CTL mobility: $1.0 \times 10^{-6} \text{ cm}^2/\text{V}\cdot\text{s}$)

Fig.13 Film thickness dependency of latent image on negatively charged OPC

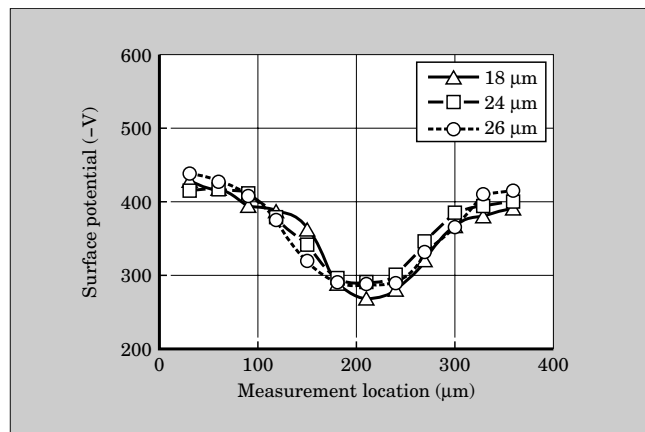
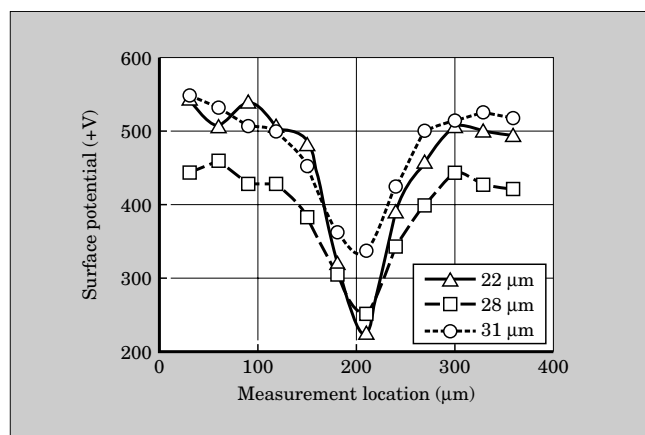


Fig.14 Film thickness dependency of latent image on positively charged OPC



- (2) Positively charged (single layer) OPC: Aluminum substrate / photoconductive layer

With the negatively charged OPC, the width of the latent image was $150 \mu\text{m}$ for a film thickness of $18 \mu\text{m}$, but the width increased to $240 \mu\text{m}$ in the case of a film thickness of $26 \mu\text{m}$. With the negatively charged multilayer OPC, an increase in film thickness due to the generation of charge at the substrate causes charge to distribute in the lateral direction, thereby decreasing resolution. These results are in agreement with prior observations.

On the other hand, the positively charged single-layer OPC has less dependency on film thickness, and for film thicknesses ranging from $22 \mu\text{m}$ to $32 \mu\text{m}$, the latent image width was narrow and ranged from 150 to $180 \mu\text{m}$. Figure 15 shows latent image widths for a negatively charged multilayer OPC and a positively charged single-layer OPC. The results support the theory that the single-layer has higher resolution because charge is generated at its surface.

3.4 Charge mobility dependency of the latent image potential

In order to investigate the correlation between the

Fig.15 Difference in latent image width due to layer structure

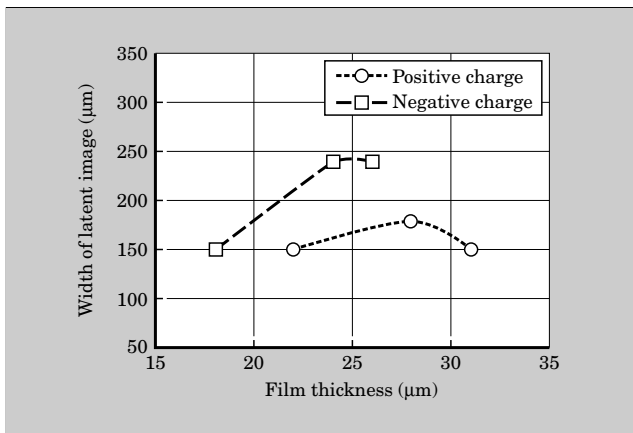
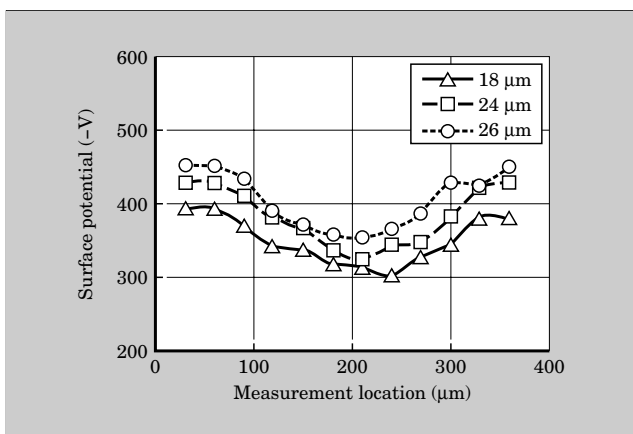


Fig.16 Latent images of high mobility CTL OPC

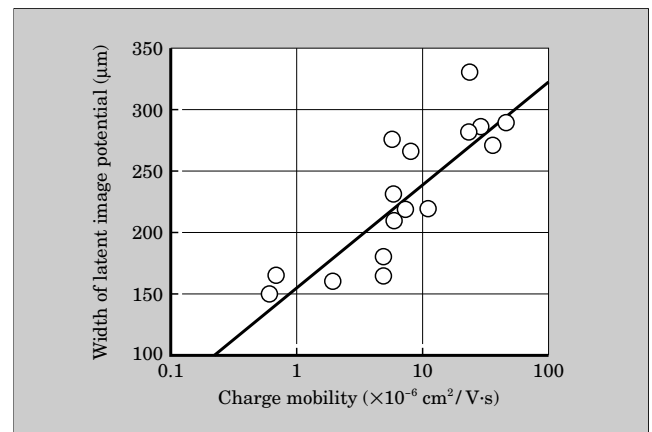


latent image shape and the electrical characteristics of the photoconductor, 1-dot latent image profiles were measured for negatively charged multilayer OPCs in which charge transport materials (CTMs) having different mobilities were used in the CTL. The CTMs used were selected for their different mobilities only, and each CTM had a different chemical structure. The mass ratio of CTM contained in the CTL to the binder was 1:1 in all cases.

Figure 16 shows the result of measurement of the latent image potential of OPC on which a CTL of even higher mobility was laminated. The CTL mobility was $1.5 \times 10^{-5} \text{ cm}^2/\text{V}\cdot\text{s}$.

In the case of the OPC of Fig. 13, at a CTL film thickness of $18 \mu\text{m}$, the latent image width was $150 \mu\text{m}$. However, in the case of the OPC on which a higher mobility CTL is laminated in Fig. 16, at a CTL film thickness of $18 \mu\text{m}$, the latent image width was $270 \mu\text{m}$. The latent image becomes wider when a higher mobility CTL is laminated. On the other hand, the latent image depth was approximately 150 V in Fig. 13 and approximately 100 V in Fig. 16, showing the OPC having the laminated layer of higher mobility CTL to have a shallower depth. The use of higher mobility CTL to support higher speed printing has opposing effects on the 1-dot latent image, its width

Fig.17 Correlation between latent image width and charge mobility on a negatively charged OPC



increases by depth decreases.

As described above, the width of the latent image is observed to increase when the film thickness of a negatively charged multilayer OPC is increased. However, the latent image potential of the negatively charged multilayer OPC is hypothesized to be dependent on the carrier mobility of charges that move within the CTL. Figure 17 shows the mobility dependency of latent image width for various types of CTMs. These experimental results confirm that increasing the mobility of the CTL causes the latent image to become wider.

The width of a 1-dot latent image on an OPC that uses a high mobility CTL is thought to be wider than in the case of using a low mobility CTL. This is in agreement with the experience thus far in which 1-dot images of low mobility CTLs have been printed as clear and sharp images.

Oka et al. have used simulations to explain that a significant deterioration in static image potential occurs when the ratio of the carrier diffusion coefficient D to the mobility μ in a CTL (D/μ) exceeds the value of 10. There is a high probability that the deterioration of a latent image is closely related to the charge transport characteristics of the CTL, and the correlation obtained in this experiment between latent image width and CTL charge mobility seems to support that relationship.

4. Conclusion

It has been reported that Fuji Electric's proprietary surface potential measurement method enables measurement of the static latent image, and several examples have been presented. Furthermore, the correlation among various parameters obtained from the MASSP signal, the photoconductive characteristics and the static latent image have been described.

In the future, Fuji Electric intends to shorten the required measurement time, to use a finer detection laser in order to achieve a more advanced 1-dot latent

image measurement device, to acquire even more detailed latent image potential profiles and to compare them to various simulated latent images in order to contribute to the development of OPCs with higher resolution.

Additionally, Fuji Electric intends to investigate the optimal exposure profile (light quantity, exposure waveform and the like) by making more flexible types of exposure lights for latent image formation and to contribute to the development of high resolution technology in the field of electrophotography.

References

- (1) Yarmchuk, E.J.;Keefe,G.E. High-resolution surface charge measurements on a organic photoconductor. *J.Appl.Phys.vol.66*, 1989, p.5435-5439.
- (2) Watanabe, Y.et al. A Numerical Study of High Resolu-

tion Latent Image Generation by Laser Beam Exposure. *IS&T's NIP 16*, 2000, p.822-826.

- (3) Chen, I. Optimization of photoreceptors for digital electrophotography. *J.Imaging Sci. and Technol.vol.34*, 1990, p.15-20.
- (4) Chen, I. Developability of interposed imagewise charge in color electrophotography.*J.Imaging Sci. and Technol.vol.35*,1991, p.365-372.
- (5) Chen, I. Electrostatic image densities in digital hybrid halftone methods. *J.Imaging Sci. and Technol.vol.39*, 1995, p.302-305.
- (6) Lin, C.W.; Nozaki, T. The measurement of Photoconductive Characteristics on Kicro-Area Surface of Photoconductor Drum. *Proceedings of IS&T's 11th International Congress on Advances in Non Impact Printing Technologies.1995*, p.138-141.

